Modulation of Electrical and Thermal Transports through Lattice Distortion in $BaTi_{1-x}Nb_xO_3$ Solid Solutions

Yuqiao Zhang[1,2,3,*], Hai Jun Cho[2], Feng Jiang[4], Chengliang Xia[5], Yue Chen[5], Weishu Liu[4,*] and Hiromichi Ohta[2,*]

[1]*Institute of Quantum and Sustainable Technology (IQST), School of Chemistry and Chemical Engineering, Jiangsu University, Zhenjiang 212013, China*

[2]*Research Institute for Electronic Science, Hokkaido University, N20W10, Kita, Sapporo 001-0020, Japan*

[3]*Foshan (Southern China) Institute for New Materials, Foshan 528200, China*

[4]*Department of Materials Science and Engineering, Southern University and Science and Technology, Shenzhen 518055, China*

[5]*Department of Mechanical Engineering, The University of Hong Kong, Pokfulam Road, Hong Kong SAR, China*

Correspondence:

Yuqiao Zhang

Institute of Quantum and Sustainable Technology (IQST), School of Chemistry and Chemical Engineering, Jiangsu University, Zhenjiang 212013, China

Research Institute for Electronic Science, Hokkaido University, N20W10, Kita, Sapporo 001-0020, Japan

Foshan (Southern China) Institute for New Materials, Foshan 528200, China

Email: yuqiaozhang0730@hotmail.com

Weishu Liu

Department of Materials Science and Engineering, Southern University and Science and Technology, Shenzhen 518055, China

Email: liuws@sustech.edu.cn

Hiromichi Ohta

Research Institute for Electronic Science, Hokkaido University, N20W10, Kita, Sapporo 001-0020, Japan

Email: hiromichi.ohta@es.hokudai.ac.jp

Abstract

The electron and heat transports in solids are through the movement of carrier electrons and quantized lattice vibrations (phonons), which are sensitive to the lattice distortion and ionized impurities, and are essential aspects for the development of novel thermoelectric materials. In this study, we systematically investigated the modulations of electrical and thermal conductivities of $BaTi_{1-x}Nb_xO_3$ solid solution (BTNO, $0 \le x \le 1$) epitaxial films. At room temperature, $BaTiO_3$ belongs to tetragonal perovskite and exhibits electron conduction through doubly degenerated Ti 3d-t_{2g} orbitals upon doping, while $BaNbO_3$ belongs to cubic perovskite and exhibits metallic electron conduction through partially filled triply degenerate Nb 4d-t_{2g} orbitals. By controlling the Ti/Nb ratio, we found a dual modulation effect on both the lattice structures and conduction band, which affects the electrical and thermal conductivities. Similar to the $SrTi_{1-x}Nb_xO_3$ solid solution (STNO, $0 \le x \le 1$) system, a phase transition was detected at $x \sim 0.5$, at which both the electron and heat transports exhibit abrupt changes. Unlike the transition in STNO, which was attributed to a polaronic phase transition, the transition in BTNO was due to contributions from both the lattice distortion and polaron effect. By controlling the lattice distortion, conduction band, and polaronic phase transitions, the electrical and thermal conductivity of BTNO epitaxial films are modulated within a much greater range than those of the STNO epitaxial films. Due to the double contribution of electron carriers and phonon to thermal conductivity (κ), the maximum κ modulation ratio of BTNO epitaxial films was ~6.9. Our research provides an effective route to design electrical/thermal management materials.

Introduction

Due to the recent increasing concern regarding the energy crisis as well as sustainability in the environment, the ability to control both electric and thermal energy is highly required, which demands an active modulation of electrical and thermal transport properties in materials [1, 2]. Electrical conductivity (σ) modulation can be realized in multiple forms, such as phase transition materials, anisotropic materials, electrical transistors, *etc*. In the case of thermal conductivity modulation (κ), it usually occurs in materials with anisotropic structures, for example, layered structures like $InGaO_3(ZnO)_m$ (m = integer)[3], layered cobalt oxides[4, 5], and SnSe[6-8], and materials with strong crystallographic textures like tungsten oxides[9, 10]. Using such approaches, Nishimura *et al.* obtained a κ modulation ratio of ~3.6 through the 3D-to-2D phase transition in nonequilibrium $(Pb_{1-x}Sn_x)Se$ solid solution[11]. However, in order to realize dual modulations of electrical and thermal transport, materials with large modulation rate in electrical conductivity (σ) which can contribute κ by Wiedemann-Franz law is required[12]. We have reported previously that in $SrTi_{1-x}Nb_xO_3$ (STNO) solid solution system, σ can be increased from 720 S cm^{-1} to 49000 S cm^{-1} with a modulation ratio of ~68, and κ can be controlled from ~6 W m^{-1} K^{-1} to ~12 W m^{-1} K^{-1} with a modulation ratio of ~2, which present a promising strategy to develop electrical and thermal management materials by the homogenous system[13, 14]. In STNO solid solution, due to the combined effects from polarons and conduction band transition, electron transport properties experienced a noticeable jump. Based on this result, we expand our design strategy for large κ modulation ratio by lattice

distortion combined with polaron/conduction band transition effects. We selected the solid solution system of $BaTi_{1-x}Nb_xO_3$ (BTNO), of which the lattice structure can be tuned through controlling Ti/Nb ratio. With a lattice structural evolution from tetragonal configuration of $BaTiO_3$ to cubic configuration of $BaNbO_3$, the electrical conductivity (σ) was modulated from ~15 S cm^{-1} to over 30000 S cm^{-1} along with a consistent jump in κ from 1.4 W m^{-1} K^{-1} to 9.6 W m^{-1} K^{-1}. The σ and κ modulation ratios can be up to ~2000 and ~6.9, respectively. Our findings will be fruitful for developing electrical/thermal management materials and devices through a homogeneous system, including thermal transistors, thermal barrier coating, thermoelectric materials, *etc*.

Experimental

Sample fabrication

High-quality $BaTi_{1-x}Nb_xO_3$ solid solution (BTNO, $0 \leq x \leq 1$) epitaxial films with thickness of ~100 nm was fabricated by pulsed laser deposition (PLD) on (001) LSAT single crystalline substrates (pseudo-cubic perovskite, a = 3.868 Å, Crystal Base Co., Ltd) using dense ceramic disks of a $BaTiO_3$–$BaNbO_3$ mixture. During growth, the substrate temperature, oxygen pressure, and laser fluence were precisely controlled at 850 °C, ~10^{-4} Pa, and 0.5 ~ 1 J cm^{-2} pulse^{-1}, yielding a growth rate of ~0.3 pm pulse^{-1}. Details of the PLD growth process of $ATi_{1-x}Nb_xO_3$ (A = alkaline earth metal elements) have been published elsewhere[13, 15, 16].

Crystallographic analyses

Crystallographic analyses of the resultant films were performed by X-ray diffraction (XRD, Cu $K\alpha_1$, ATX-G, Rigaku Co.). All the samples show a sharp out-of-plane rocking curve with a full width at half maximum (FWHM) of 0.02 ~ 0.03° (≡ resolution of the Ge 220 two crystal monochrometer configuration), suggesting a highly aligned lattice with a low degree of mosaic spread along the cross-plane direction (**Figure S1**).

Electron transport property measurements

Electrical conductivity (σ), carrier concentration (n), and Hall mobility (μ_{Hall}) were measured at room temperature and low temperature by a conventional d.c. four-probe method using an In–Ga alloy as the electrodes with van der Pauw geometry. Thermopower (S) was measured at room temperature by a conventional steady-state method. Temperature difference (ΔT) of ~4 K across the film was created by using two Peltier devices while using two small thermocouples to monitor the actual temperatures of each end of the $BaTi_{1-x}Nb_xO_3$ films. The thermo-electromotive force (ΔV) and ΔT were measured simultaneously, and S-values were obtained from the slope of the ΔV–ΔT plots. We measured 2-3 samples for each composition to check the accuracy.

Thermal conductivity measurement

The thermal conductivity (κ) was calculated from $\kappa = \alpha \cdot C_p \cdot \rho$, where α is the thermal diffusivity, C_p is the specific heat, and ρ is the density of the sample. The C_p of the samples was measured by laser flash method (LFA457 *MicroFlash*®, NETZSCH Co.[17]) at room temperature. The α along the cross-plane direction of $BaTi_{1-x}Nb_xO_3$ epitaxial films

was measured by time-domain thermoreflectance (TDTR) methods (Front heating/Front detection mode-Mirror image method, PicoTR, PicoTherm Co., uncertainty ≤ ±6.2 %[18]). In order to reduce measurement errors due to the uniformity of samples, the thermal conductivity results were averaged by multiple checks at different areas of each sample. And we checked the deviation is enough small by measuring 2-3 samples in each composition.

DFT calculation

Density of states (DOS) of $BaTi_{1-x}Nb_xO_3$ solid solutions was calculated using the Korringa-Kohn-Rostoker (KKR) method and the coherent potential approximation (CPA) within the AkaiKKR (Machikaneyama) package[19, 20]. The parametrization of the exchange-correlation energy in the form of Perdew-Burke-Ernzerhof was used[21]. Dense meshes with 1183 and 1800 **k**-points were used for self-consistent and DOS calculations, respectively. In the KKR-CPA calculations, experimental lattice constants of $BaTi_{1-x}Nb_xO_3$ were used. The atomic positions of *P*4*mm* $BaTi_{0.95}Nb_{0.05}O_3$ follow the experimental values of *P*4*mm* $BaTiO_3$[22].

Results and discussion

$BaTiO_3$ is an insulating tetragonal perovskite with spontaneous polarization induced by the deformation of TiO_6 octahedra, while $BaNbO_3$ is a metallic cubic perovskite with highly conductive Nb 4d band (**Figure 1**). Therefore, we speculate that by controlling the Ti/Nb ratio, there will be a tetragonal-to-cubic lattice transition along with Ti 3d-to-Nb 4d conduction band shift, which is possible to modulate the electrical and thermal

transports within a wide range.

To confirm our hypothesis, $BaTi_{1-x}Nb_xO_3$ solid solution (BTNO, $0 \le x \le 1$) epitaxial films were fabricated on (001) LSAT single crystal substrates. **Figure 2(a)** summarizes the changing pattern of reciprocal space mapping (RSM) diffraction spots for the BTNO epitaxial films (original RSM are shown in **Figure S2**). All films were incoherently and heteroepitaxially grown with a fully relaxed lattice on the substrates [LSAT, $(q_x/2\pi,\ q_z/2\pi) = (-2.64,\ 7.76)\ nm^{-1}$]. Directly reflected in the RSM, the diffraction spots of BTNO deviates obviously from the cubic line at $x \le 0.3$, indicating a lattice distortion. Using the $\bar{1}03$ diffraction spots, the lattice parameters were calculated ($a = -20\pi/q_x$ Å, $c = 60\pi/q_z$ Å), which is plotted in **Figure 2(b)** versus x. All the samples show a stable average lattice constant [i.e. $(a^2c)^{1/3}$] around the tendency predicted by Vegard's law, which was calculated assuming cubic lattice for all the compositions. However, from the a/c ratio, great tetragonal distortion could be found in samples at $0 \le x < 0.3$ [**Figure 2(c)**]. In case of pure $BaTiO_3$ ($x = 0$), the a/c value is below 1, indicating an enlarged lattice along the out-of-plane direction. At room temperature, $BaTiO_3$ has the tetragonal structure. In the thin film case, its orientation depends on background pressure during deposition[23]. During our experiments with the background pressure of $\sim 10^{-4}$ Pa, $BaTiO_3$ selectively grows along the polarized direction, resulting in an enlarged c axis. As Nb substitutes the Ti-site, a/c values show an abrupt increase above 1, indicating the orientation has been rotated by 90° from the out-of-plane to the in-plane direction. In the $BaTiO_3$ system, Nb substitution at Ti-site

improved polarization fatigue resistance and remnant polarization through tilting the oxygen octahedra[24-26]. With increasing Nb substitution, *a*/*c* exhibits a decreasing tendency and finally returns to ~1 at $x \geq 0.3$, suggesting a structural transition from tetragonal perovskite to cubic perovskite. Hereafter, a stable cubic structure was kept for all the compositions.

After Nb substitution, the tilted orientation will result in the polarization aligning along the in-plane direction, which can be directly reflected in the increasing electron scatterings. As shown in **Figure 3(a-d)**, electrical properties, including electrical conductivity (σ), carrier concentration (n), Hall mobility (μ_{Hall}), and thermopower (S), are measured and plotted versus x in comparison with STNO epitaxial films[13]. σ displays an overall similar increasing tendency of BTNO epitaxial films compared with STNO epitaxial films. However, the σ values of BTNO epitaxial films at $x \leq 0.5$ are much lower than those of STNO epitaxial films while at $x > 0.5$, they jump to a similar level [**Figure 3(a)**]. In both cases, the n values follow the nominal tendency in the same way [**Figure 3(b)**]. Therefore, the difference in σ is decided by μ_{Hall} ($\sigma = e \cdot n \cdot \mu_{\mathrm{Hall}}$). As shown in **Figure 3(c)**, at $x \leq 0.5$ μ_{Hall} firstly increases and then decreases with x, holding values lower than those of STNO epitaxial films. At $x > 0.5$, similar to STNO epitaxial films, a sharp jump in μ_{Hall} is detected, and the values return to the same level as STNO. Comparing BTNO and STNO epitaxial films at $x < 0.5$, there are several reasons accounting for the different μ_{Hall} values. At $x < 0.3$, obvious tetragonal distortion along the in-plane direction exists in BTNO epitaxial films, while STNO epitaxial films hold

the stable cubic structure. The polarization along the in-plane direction will limit the μ_{Hall}. Consistent with the decreasing tetragonal distortion, there is a quick increase in μ_{Hall} of BTNO epitaxial films. Although the tetragonal distortion disappears at $x \geq 0.3$, μ_{Hall} of BTNO epitaxial films is still below that of STNO epitaxial films and decrease a little between $x = 0.4$ and 0.5. This may be due to the different polaron effects at the Ti^{3+}/Ti^{4+} sight and ionic scattering from alloying Nb and Ti in the system. As $x > 0.5$, a jump similar to that of STNO epitaxial films was observed in μ_{Hall} of BTNO epitaxial films, indicating a similar polaronic phase boundary at $x \sim 0.5$[14]. And with further increasing Nb substitution, μ_{Hall} displays a steady increasing tendency. To develop deeper insights into the electron transport properties of BTNO system, we measured the thermopower (S) and calculated density of states effective mass (m^*_{DOS}) using S and n based on equations (1) to (3) with the relation of relaxation time (τ) and carrier energy (E) expressed as $\tau \propto E^{r-0.5}$[13, 15], from which the electron effective mass ($m^* = m^*_{DOS}$ / electronic degree of freedom) was deduced:

$$S = \frac{k_B}{e}\left[\frac{(1+s+r)F_{s+r}(\eta)}{(s+r)F_{s+r-1}(\eta)} - \eta\right] \quad (1)$$

where k_B, n, r, and F_r are the Boltzmann constant, chemical potential, scattering parameter of relaxation time, and Fermi integral, respectively. Here, the s value is 1 which is for 3D system[27]. F_r is given by

$$F_r(\xi) = \int_0^\infty \frac{x^r}{1+e^{x-\xi}}\,dx \quad (2)$$

and n is given by

$$n = 4\pi\left(\frac{2m^*_{DOS}k_BT}{h^2}\right)^{\frac{3}{2}} F_{\frac{1}{2}}(\xi) \quad (3)$$

where h and T are the Planck constant and absolute temperature, respectively. Here, the main scattering channel is from the polar optical phonons, so r value is selected to be 0.5[28]. **Figure 3(d)** shows that $-S$ follows a general decreasing tendency with Nb substitution due to the increasing n. However, different from STNO epitaxial films, when $-S$ is plotted versus n, the slope of the pattern is larger than 198 μV K^{-1} $decade^{-1}$, which suggests a varying m^* with Nb substitution [inset of **Figure 3(d)**][29]. The m^* of BTNO epitaxial films shows a gradual decrease with Nb substitution at $x < 0.3$ and then keeps constant before another slight decrease at $x > 0.8$ [**Figure 3(e)**]. The gradual decrease of m^* in BTNO epitaxial films, which is different from the step-like decrease due to the transition of conduction band from Ti 3d to Nb 4d in STNO, is well consistent with the evaluation of lattice distortion from tetragonal to cubic structure, suggesting that tetragonal distortion induced polarization results in the enhanced m^*. Furthermore, electron relaxation time, τ, was extracted ($\tau = \mu_{Hall} \cdot m^* \cdot e^{-1}$) from μ_{Hall} and m^* [**Figure 3(f)**]. Following the tendency of μ_{Hall}, τ displays firstly increasing and then decreasing tendency with Nb substitution at $x \leq 0.5$ with much lower values than those of STNO epitaxial films. However, at $x > 0.5$, τ returns to the similar values of STNO epitaxial films. Therefore, in BTNO epitaxial films, the electron scattering is not only from ionic Nb dopant but also predominantly from the in-plane polarization triggered by tetragonal distortion.

Figure 4 shows the temperature-dependent resistivity and Seebeck coefficient of BTNO epitaxial films were measured within the temperature range of 10 K to 300 K,

suggesting a strong dependence on the lattice distortion. An insulator-to-metal transition happens at $x > 0.2$ ($n \sim 4.5 \times 10^{21}$ cm^{-3}). In addition, except for BTNO film at $x = 0.05$, S of all other samples show a monotonously decreasing tendency towards the low temperature, which suggests a constantly metallic behavior[30]. In this case, Fermi level is located within a band of allowed electron states with transport occurring in the vicinity of Fermi energy (E_F), which is similar to the La-doped $BaTiO_3$[30, 31]. The metallic behavior of S suggests an almost constant n in BTNO with temperature. Therefore, at $x \leq 0.2$, the constant n accompanied by a thermally activated ρ indicates a thermally activated μ_{Hall} which originates from the electron localization[30]. Similar behavior was also reported by other researchers both in La/Nb doped and oxygen-deficient $BaTiO_3$, where a small polaron hopping of conduction mechanism was deduced[31-34]. In contrast, the μ_{Hall} of STNO system is limited by large polarons[14]. The lattice distortion in BTNO will bring a much stronger trapping potential for carriers, resulting in the formation of small polarons. The polaron hopping conduction could also be reflected by x dependent electron mean free path (l_e, **Figure S3**). At $x \leq 0.5$, l_e is much shorter than the lattice constant, suggesting a polaron hopping conduction mechanism. On the contrary, at $x \geq 0.6$, l_e jumps beyond the lattice constant, which is expected from band conduction. Therefore, in BTNO case, the main electron scattering is supposed to be from polarization induced by tetragonal distortions. It is worth noting that BTNO at $x = 0.05$ displays a changing of S values from negative to positive at $T <$ 80 K, which is consistent with a Mott-Hubbard insulator description revealed in rare-earth-doped $BaTiO_3$ and $SrTiO_3$[35-38].

Furthermore, we calculated the electronic structure of BTNO at x = 0, 0.05, 0.3, 0.5, 0.6, 0.8 and 1. In order to reproduce the real lattice configuration, the measured lattice constants were used. **Figure 5** summarizes the projected density of states (DOS) of BTNO around the bandgap. The energy origin was set at the Fermi level (E_F). The E_F locates within the bandgap for pristine $BaTiO_3$, therefore $BaTiO_3$ shows insulating nature. With Nb substitution at the Ti site, E_F tends to increase and locates deep in the conduction band. In BTNO at x = 0.05, the conduction is mainly dependent on Ti 3d conduction band while Nb 4d conduction band makes major contributions in BTNO at $x \geq 0.3$, which is consistent with the m^* changing pattern.

From the Wiedemann-Franz law, it can be found that electron transport will contribute to κ by:

$$\kappa = \kappa_{lat} + L\sigma T \tag{4}$$

where κ_{lat} is lattice thermal conductivity mainly dependent on propagation of lattice vibrations, L is Lorenz number and T is absolute temperature. For free electron systems, $L_0 = \frac{\pi^2 k_B^2}{3e^2} \sim 2.44 \times 10^{-8}\ V^2\ K^{-2}$, where k_B is Boltzmann constant. However, for most of the semiconductors, the real L is generally lower than $2.44 \times 10^{-8}\ V^2\ K^{-2}$. Based on the reduced Fermi energy ($\xi = E_F/k_BT$) and scattering parameter (r), the real L could be calculated as follows[39, 40]:

$$L = \left(\frac{k_B}{e}\right)^2 \left\{ \frac{(r+3)F_{r+2}(\xi)}{(r+1)F_r(\xi)} - \left[\frac{(r+2)F_{r+1}(\xi)}{(r+1)F_r(\xi)}\right]^2 \right\} \tag{5}$$

where $F_n(\xi)$ is the Fermi integration

$$F_n(\xi) = \int_0^\infty \frac{x^n}{1 + e^{x-\xi}} \mathrm{d}x \tag{6}$$

The ξ value can be derived from the in-plane S values based on single band approximation,

$$S = \pm \frac{k_B}{e} \left[\frac{(r+2)F_{r+1}(\xi)}{(r+1)F_r(\xi)} - \xi \right] \tag{7}$$

In BTNO system, due to the lattice evolution (conduction band shift and polaronic phase transition), σ can be modulated from ~15 S cm^{-1} to over 30000 S cm^{-1}, which suggests an electron contribution to κ from 0.08 W m^{-1} K^{-1} to 24 W m^{-1} K^{-1} [κ_{ele}, **Figure 6(a)**]. Therefore, it is possible to obtain a large κ modulation ratio in BTNO system. We then measured the cross-plane κ of BTNO epitaxial films by TDTR method. As shown in **Figure 6(b)**, the κ follows a similar changing pattern to that of κ_{ele}, suggesting a large contribution from electrons to the thermal transport. However, comparing κ_{ele} and κ, it could be found that κ is much lower than κ_{ele} in BTNO at $x \geq 0.6$, even though the lattice structure is isotropic along the in-plane and cross-plane directions. A similar phenomenon was also found in STNO system[14]. This may be due to the different measurement directions of σ and κ, which results in a different scattering rate for electrons and phonons. Furthermore, other intrinsic properties of materials can also result in less contribution from electrons to thermal transport, such as “non-Fermi liquid behavior”[41], “hydrodynamic regime”[42], “quantum critical point”[43], *etc*., which is still to be explored. However, the highly consistent behaviors of σ and κ suggests a coupling between electrical and thermal transports in BTNO

system. In addition, the lattice structure also affects phonon transport which contributes to κ in form of κ_{lat}. With lattice distortion phonon transfer will be hindered, resulting in much lower κ values. Similar phenomenon was also reported in $Sr_{1-x}La_xTiO_3$ solid solution system[14]. With the large modulation ratio of electron and phonon transports, the κ modulation ratio can reach ~6.9 by controlling Nb substitution.

Based on the electrical and thermal transport properties of STNO and BTNO systems, it can be found that in titanates transport properties are highly dependent on lattice distortion and conduction band. Both systems display intrinsic conduction band transition from Ti 3d to Nb 4d at $x \sim 0.3$. However, attributed to the different lattice structures, Ti 3d-t_{2g} orbital of STNO has double degeneracy while Ti 3d-t_{2g} orbital of BTNO has triple degeneracy. Accordingly, the m^* of electrons in BTNO is much large than that in STNO, which contributes to enhancing S. If we consider thermoelectric applications, this is good news to have large S values. However, on the other hand, tetragonal distortion induced spontaneous polarization in BTNO system will constrain electron transport, resulting in deteriorated σ and power factor ($PF = S^2 \cdot \sigma$). In this case, BTNO shows much lower thermoelectric performance than STNO. Even so, substituting Ba at Sr-site still provides us with much lower κ (~4 times lower of $BaTiO_3$ than $SrTiO_3$), suggesting a strategy to balance electrical and thermal transports through modifying lattice distortion degree. Sublattice alloying induced structure distortion could be an effective strategy to tune the transport of electrons and phonons, benefit the application of thermoelectric conversion, thermal transistors, and thermal barrier

coating.

Conclusion

In summary, we have clarified the electron and heat transport properties of BTNO epitaxial films at room temperature. Due to the lattice structural evolution, conduction band shift as well as polaronic phase transition, BTNO system displays large modulation ratios in both σ and κ with Nb substitution. The changing pattern of κ is highly consistent with that of σ, suggesting an important contribution from electrons to heat transport. With Nb substitution for Ti, σ increases from ~15 S cm^{-1} to over 30000 S cm^{-1} along with κ increasing from 1.4 W m^{-1} K^{-1} to 9.6 W m^{-1} K^{-1}, resulting in large σ and κ modulation ratios of ~2000 and ~6.9, respectively. Our findings will present in accordance to designing electrical/thermal management materials, such as thermoelectric materials.

Acknowledgments

This research was supported by Grants-in-Aid for Innovative Areas (19H05791). Y.Z acknowledges the support of the International Research Fellowship from the JSPS (19F19049), the Start-Up Fund of Jiangsu University (5501310015), Guangdong Basic and Applied Basic Research Foundation (2021A1515110881), and the Youth fund of Foshan (Southern China) Institute for New Materials (2021AYF25009). H.J.C. acknowledges the support from Nippon Sheet Glass Foundation for Materials Science and Engineering. H.O. was supported by Grants-in-Aid for Scientific Research A

(22H00253). W.S.L acknowledges the support of Shenzhen Key Projects of Long-Term Academic Support Plan 20200925164021002. C.X and Y.C are grateful for the research computing facilities offered by ITS, HKU.

Data availability statement

All data that support the findings of this study are included within the article (and any supplementary files).

Conflicts of interest

The authors declare no competing financial interest.

Reference

[1] Li N B, Ren J, Wang L, Zhang G, Hanggi P and Li B W 2012 Colloquium: Phononics: Manipulating heat flow with electronic analogs and beyond *Rev Mod Phys* **84** 1045-66

[2] Wehmeyer G, Yabuki T, Monachon C, Wu J Q and Dames C 2017 Thermal diodes, regulators, and switches: Physical mechanisms and potential applications *Appl Phys Rev* **4** 041304

[3] Cho H J, Wu Y Z, Zhang Y Q, Feng B, Mikami M, Shin W, Ikuhara Y, Sheu Y M, Saito K and Ohta H 2021 Anomalously Low Heat Conduction in Single-Crystal Superlattice Ceramics Lower Than Randomly Oriented Polycrystals *Adv Mater Interfaces* **8** 2001932

[4] Takashima Y, Zhang Y-q, Wei J, Feng B, Ikuhara Y, Cho H J and Ohta H 2021 Layered cobalt oxide epitaxial films exhibiting thermoelectric *ZT* = 0.11 at room temperature *Journal of Materials Chemistry A* **9** 274-80

[5] Cho H J, Takashima Y, Nezu Y, Onozato T and Ohta H 2020 Anisotropic Heat Conduction in Ion-Substituted Layered Cobalt Oxides *Adv Mater Interfaces* **7** 1901816

[6] Chang C, Wu M H, He D S, Pei Y L, Wu C F, Wu X F, Yu H L, Zhu F Y, Wang K D, Chen Y, Huang L, Li J F, He J Q and Zhao L D 2018 3D charge and 2D phonon transports leading to high out-of-plane *ZT* in n-type SnSe crystals *Science* **360** 778-82

[7] Su L, Wang D, Wang S, Qin B, Wang Y, Qin Y, Jin Y, Chang C and Zhao L-D 2022 High thermoelectric performance realized through manipulating layered phonon-electron decoupling *Science* **375** 1385-9

[8] Zhao L-D, Lo S-H, Zhang Y, Sun H, Tan G, Uher C, Wolverton C, Dravid V P and Kanatzidis M G 2014 Ultralow thermal conductivity and high thermoelectric figure of merit in SnSe crystals *Nature* **508** 373-7

[9] Kim G, Feng B, Ryu S, Cho H J, Jeen H, Ikuhara Y and Ohta H 2021 Anisotropic Electrical Conductivity of Oxygen-Deficient Tungsten Oxide Films with Epitaxially Stabilized 1D Atomic Defect Tunnels *Acs Appl Mater Inter* **13** 6864-9

[10]Kim G, Feng B, Sheu Y M, Cho H J, Ikuhara Y and Ohta H 2020 Coexistence of High Electron Conduction and Low Heat Conduction in Tungsten Oxide Epitaxial Films with 1D Atomic Defect Tunnels *Acs Appl Electron Ma* **2** 2507-13

[11]Nishimura Y, He X, Katase T, Tadano T, Ide K, Kitani S, Hanzawa K, Ueda S, Hiramatsu H, Kawaji H, Hosono H and Kamiya T 2022 Electronic and Lattice Thermal Conductivity Switching by 3D−2D Crystal Structure Transition in Nonequilibrium $(Pb_{1-x}Sn_x)Se$ *Advanced Electronic Materials* 2200024

[12]Franz R and Wiedemann G 1853 Ueber die Wärme-Leitungsfähigkeit der Metalle *Annalen der Physik* **165** 497-531

[13]Zhang Y Q, Feng B, Hayashi H, Tohei T, Tanaka I, Ikuhara Y and Ohta H 2017 Thermoelectric phase diagram of the $SrTiO_3$-$SrNbO_3$ solid solution system *Journal of Applied Physics* **121** 185102

[14]Zhang Y Q, Cho H J, Sugo K, Mikami M, Woo S, Jung M C, Zhuang Y H, Bin F, Sheu Y M, Shin W, Choi W S, Han M J, Ikuhara Y and Ohta H 2021 Low thermal conductivity of $SrTiO_3$-$LaTiO_3$ and $SrTiO_3$-$SrNbO_3$ thermoelectric oxide solid solutions *J Am Ceram Soc* **104** 4075-85

[15]Zhang Y, Sugo K, Cho H J and Ohta H 2019 Thermoelectric phase diagram of the $SrTiO_3$-$LaTiO_3$ solid-solution system through a metal to Mott insulator transition *Journal of Applied Physics* **126** 075104

[16]Zhang Y Q, Feng B, Hayashi H, Chang C P, Sheu Y M, Tanaka I, Ikuhara Y and Ohta H 2018 Double thermoelectric power factor of a 2D electron system *Nat Commun* **9** 1-7

[17]Min S, Blumm J and Lindemann A 2007 A new laser flash system for measurement of the thermophysical properties *Thermochim Acta* **455** 46-9

[18]Firoz S H, Yagi T, Taketoshi N, Ishikawa K and Baba T 2011 Direct observation of thermal energy transfer across the thin metal film on silicon substrates by a rear

heating-front detection thermoreflectance technique *Meas. Sci. Technol.* **22** 024012

[19]Tulip P R, Staunton J B, Lowitzer S, Kodderitzsch D and Ebert H 2008 Theory of electronic transport in random alloys with short-range order: Korringa-Kohn-Rostoker nonlocal coherent potential approximation *Phys Rev B* **77** 165116

[20]Akai H 1989 Fast Korringa-Kohn-Rostoker coherent potential approximation and its application to FCC Ni-Fe systems *Journal of Physics: Condensed Matter* **1** 8045-64

[21]Perdew J P, Burke K and Ernzerhof M 1996 Generalized Gradient Approximation Made Simple *Physical Review Letters* **77** 3865-8

[22]Terauchi H, Watanabe Y, Kasatani H, Kamigaki K, Yano Y, Terashima T and Bando Y 1992 Structural Study of Epitaxial $BaTiO_3$ Crystals *Journal of the Physical Society of Japan* **61** 2194-7

[23]Lyu J K, Estandia S, Gazquez J, Chisholm M F, Fina I, Dix N, Fontcuberta J and Sanchez F 2018 Control of Polar Orientation and Lattice Strain in Epitaxial $BaTiO_3$ Films on Silicon *Acs Appl Mater Inter* **10** 25529-35

[24]Bhide V G, Hegde M S and Deshmukh K G 1968 Ferroelectric Properties of Lead Titanate *J Am Ceram Soc* **51** 565-8

[25]Kim J K, Kim J, Song T K and Kim S S 2002 Effects of niobium doping on microstructures and ferroelectric properties of bismuth titanate ferroelectric thin films *Thin Solid Films* **419** 225-9

[26]Co K, Sun F-C, Alpay S P and Nayak S K 2019 Polarization rotation in $Bi_4Ti_3O_{12}$ by isovalent doping at the fluorite sublattice *Phys Rev B* **99** 014101

[27]Durczewski K and Ausloos M 2000 Nontrivial behavior of the thermoelectric power: Electron-electron versus electron-phonon scattering *Phys Rev B* **61** 5303-10

[28]Ohta S, Nomura T, Ohta H and Koumoto K 2005 High-temperature carrier transport and thermoelectric properties of heavily La- or Nb-doped SrTiO3 single crystals *Journal of Applied Physics* **97** 034106

[29]Ohta H, Kim S, Mune Y, Mizoguchi T, Nomura K, Ohta S, Nomura T, Nakanishi

Y, Ikuhara Y, Hirano M, Hosono H and Koumoto K 2007 Giant thermoelectric Seebeck coefficient of a two-dimensional electron gas in $SrTiO_3$ *Nature Materials* **6** 129-34

[30]Mott N F and Davis E A 2012 *Electronic processes in non-crystalline materials*: Oxford university press)

[31]Gilbert S R, Wills L A, Wessels B W, Schindler J L, Thomas J A and Kannewurf C R 1996 Electrical transport properties of epitaxial $BaTiO_3$ thin films *Journal of Applied Physics* **80** 969-77

[32]Liu L, Guo H, Lü H, Dai S, Cheng B and Chen Z 2005 Effects of donor concentration on the electrical properties of Nb-doped $BaTiO_3$ thin films *Journal of Applied Physics* **97** 054102

[33]Kolodiazhnyi T, Tachibana M, Kawaji H, Hwang J and Takayama-Muromachi E 2010 Persistence of Ferroelectricity in $BaTiO_3$ through the Insulator-Metal Transition *Physical Review Letters* **104** 147602

[34]Kolodiazhnyi T 2008 Insulator-metal transition and anomalous sign reversal of the dominant charge carriers in perovskite$BaTiO_{3-\delta}$ *Phys Rev B* **78** 045107

[35]Hudson L T, Kurtz R L, Robey S W, Temple D and Stockbauer R L 1993 Photoelectron Spectroscopic Study of the Valence and Core-Level Electronic-Structure of $BaTiO_3$ *Phys Rev B* **47** 1174-80

[36]Robey S W, Hudson L T, Eylem C and Eichorn B 1993 Substitution-Induced Midgap States in the Mixed Oxides $R_xBa_{1-x}TiO_3$-Delta with R = Y, La, and Nd *Phys Rev B* **48** 562-8

[37]Fujimori A, Hase I, Nakamura M, Namatame H, Fujishima Y, Tokura Y, Abbate M, Degroot F M F, Czyzyk M T, Fuggle J C, Strebel O, Lopez F, Domke M and Kaindl G 1992 Doping-Induced Changes in the Electronic-Structure of $La_xSr_{1-x}TiO_3$ - Limitation of the One-Electron Rigid-Band Model and the Hubbard-Model *Phys Rev B* **46** 9841-4

[38]Fujimori A, Hase I, Tokura Y, Abbate M, Degroot F M F, Fuggle J C, Eisaki H and Uchida S 1993 Evolution of the Spectral-Function in Mott-Hubbard Systems across

Metal-Insulator Transitions *Physica B* **186-88** 981-5

[39]Bhandari D R C and Rowe D 1983 Modern thermoelectrics *Holt, Riehart and Winston, London*

[40]Kim H S, Gibbs Z M, Tang Y L, Wang H and Snyder G J 2015 Characterization of Lorenz number with Seebeck coefficient measurement *APL Mater.* **3** 041506

[41]Kim K S and Pepin C 2009 Violation of the Wiedemann-Franz Law at the Kondo Breakdown Quantum Critical Point *Physical Review Letters* **102** 156404

[42]Lee S, Hippalgaonkar K, Yang F, Hong J W, Ko C, Suh J, Liu K, Wang K, Urban J J, Zhang X, Dames C, Hartnoll S A, Delaire O and Wu J Q 2017 Anomalously low electronic thermal conductivity in metallic vanadium dioxide *Science* **355** 371-4

[43]Jaoui A, Fauque B, Rischau C W, Subedi A, Fu C G, Gooth J, Kumar N, Suss V, Maslov D L, Felser C and Behnia K 2018 Departure from the Wiedemann-Franz law in WP2 driven by mismatch in T-square resistivity prefactors *Npj Quantum Mater* **3** 1-7

Figures and captions

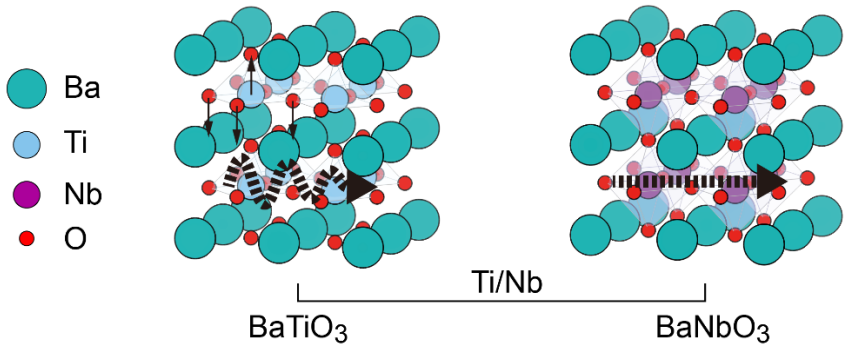

Figure 1. Schematic crystal structures for $BaTiO_3$ and $BaNbO_3$. Through controlling Ti/Nb ratio, crystal structure and electron conduction mechanism are possible to be tuned in $BaTi_{1-x}Nb_xO_3$ ($0 \leq x \leq 1$) solid solution system.

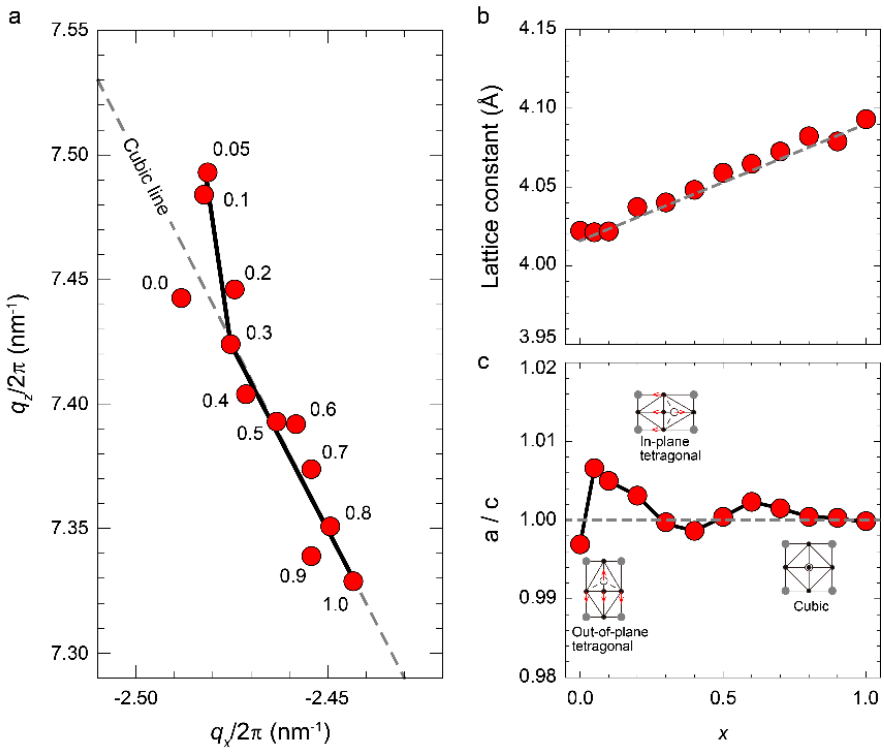

Figure 2. Crystallographic characterization of the $BaTi_{1-x}Nb_xO_3$ ($0 \le x \le 1$, BTNO) epitaxial films on LSAT single crystal substrate at room temperature. (a) Schematic illustrations of X-ray reciprocal space mappings around the $\bar{1}03$ diffraction spot of the BTNO epitaxial films. Red symbols indicate the peak positions of the BTNO epitaxial films. (b) x dependent average lattice constant of the BTNO epitaxial films [$= (a^2 \cdot c)^{1/3}$]. The average lattice constant shows an increasing tendency, following Vegard's law (grey dash line). (c) x dependent a/c value of BTNO epitaxial films. Obvious tetragonal distortion occurs at $x < 0.3$, while samples at $x \ge 0.3$ stay at a cubic structure. The lattice polarization is indicated by the red arrows schematically, which display a transition from out-of-plane direction to in-plane direction with Nb substitution.

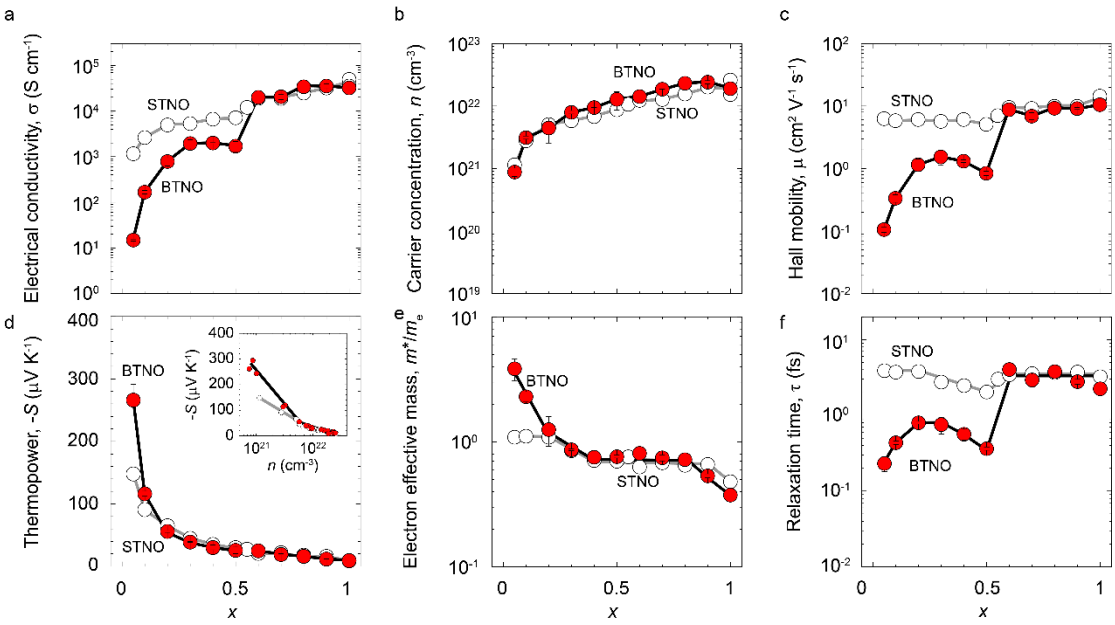

Figure 3. Room temperature electron transport properties of $BaTi_{1-x}Nb_xO_3$ solid solution ($0 \leq x \leq 1$, BTNO) epitaxial films in comparison with those of $SrTi_{1-x}Nb_xO_3$ solid solution ($0 \leq x \leq 1$, STNO) epitaxial films[13]. (a) Electrical conductivity (σ), (b) carrier concentration (n), (c) Hall mobility (μ_{Hall}), (d) thermopower ($-S$), (e) electron effective mass (m^*), (f) relaxation time (τ). The black and grey lines are drawn as visual guidance.

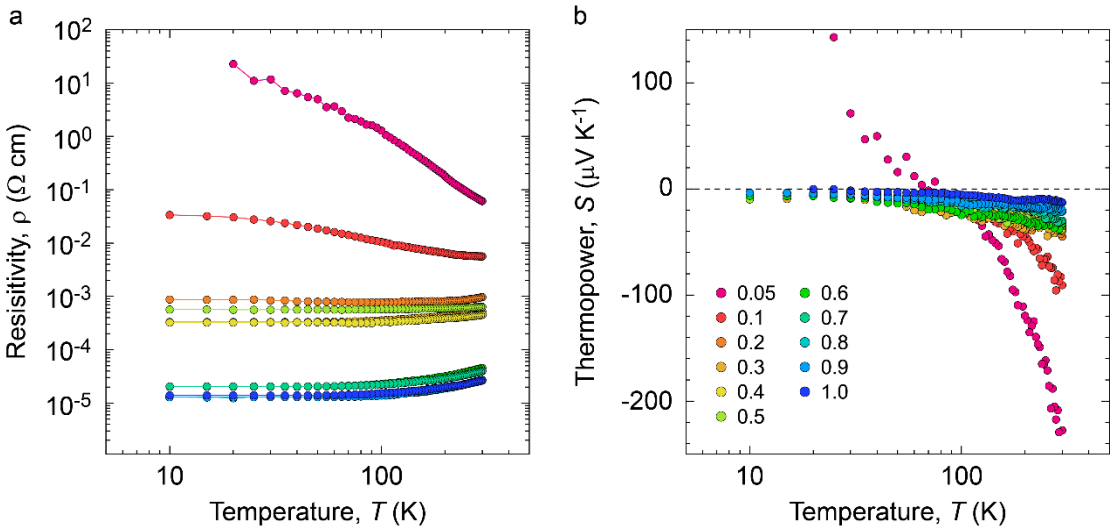

Figure 4. Temperature dependence of (a) resistivity (ρ) and (b) thermopower (S) of the $BaTi_{1-x}Nb_xO_3$ solid solution ($0 \leq x \leq 1$, BTNO) epitaxial films. Insulating/semiconducting-to-metallic transition is observed at $x \sim 0.2$ from the ρ–T curves, while S–T changing pattern follows metallic behavior for all the compositions.

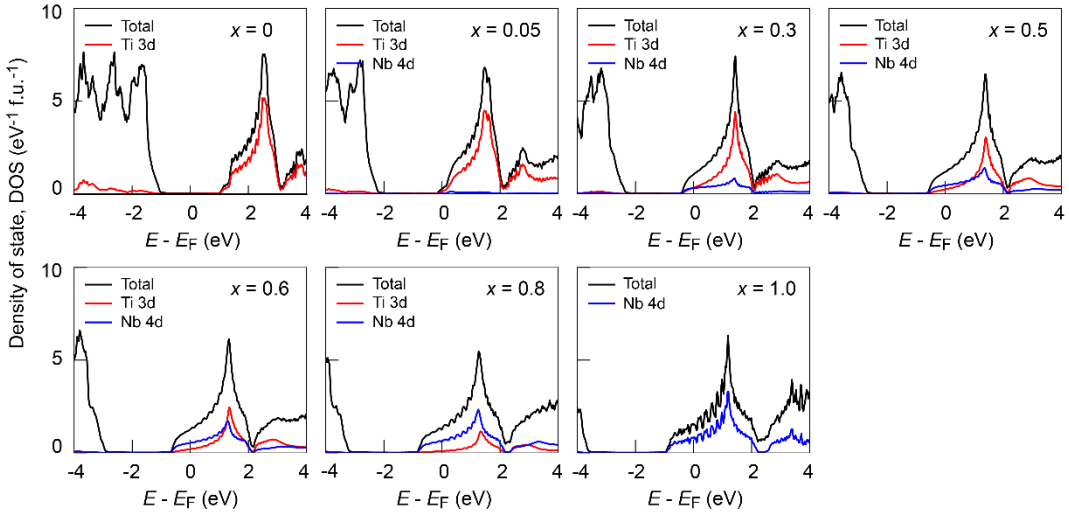

Figure 5. Calculated density of states (DOS) for $BaTi_{1-x}Nb_xO_3$ (BTNO, $x = 0$, 0.05, 0.3, 0.5, 0.6, 0.8 and 1.0) solid solutions. The energy origin was set at the Fermi level E_F. Nb 4d states make major contributions to the DOS near the conduction band edge when x is above 0.3. Lattice constants a and c of $P4mm$ $BaTiO_3$ are 4.019 Å and 4.031 Å, respectively. Lattice constants a and c of $P4mm$ $BaTi_{0.95}Nb_{0.05}O_3$ are 4.03 Å and 4.001 Å, respectively. Lattice constants of $Pm\bar{3}m$ $BaTi_{0.7}Nb_{0.3}O_3$, $BaTi_{0.5}Nb_{0.5}O_3$, $BaTi_{0.4}Nb_{0.6}O_3$, $BaTi_{0.2}Nb_{0.8}O_3$, and $BaNbO_3$ are 4.04 Å, 4.06 Å, 4.068 Å, 4.083 Å, and 4.093 Å, respectively.

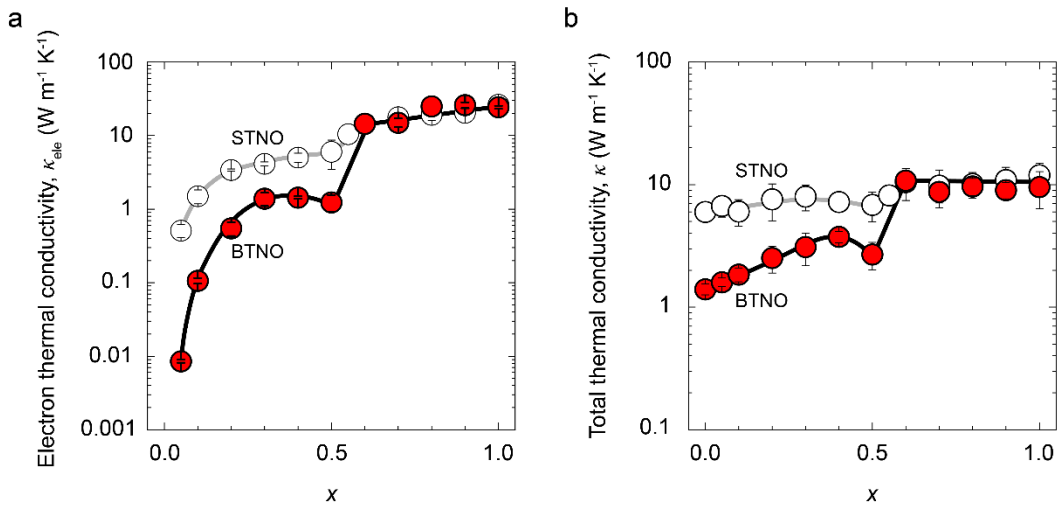

Figure 6. x dependent (a) electron thermal conductivity (κ_{ele}) and (b) total thermal conductivity (κ) of $BaTi_{1-x}Nb_xO_3$ solid solution (BTNO, $0 \leq x \leq 1$) epitaxial films (red symbols) at room temperature in comparison with those of $SrTi_{1-x}Nb_xO_3$ solid solution (STNO, $0 \leq x \leq 1$) epitaxial films (white symbols)[14].